Hybridization of additive manufacturing processes to build ceramic/metal parts: Example of HTCC

Jonathan Raynaud, Vincent Pateloup, Mégane Bernard, Delphine Gourdonnaud, Damien Passerieux, Dominique Cros, Valérie Madrangeas, Philippe Michaud, Thierry Chartier

Hybridization of additive manufacturing processes to build ceramic/metal parts: example of HTCC

Jonathan Raynaud[1], Vincent Pateloup[1], Mégane Bernard[1], Delphine Gourdonnaud[1], Damien Passerieux[2], Dominique Cros[2], Valérie Madrangeas[2], Philippe Michaud[1], Thierry Chartier[1]

[1] *CNRS, University of Limoges, Institute of Research for Ceramics (IRCER), UMR 7315, European Ceramics Center, Limoges, France*

[2] *CNRS, University of Limoges, XLim, UMR 7252, Limoges, France*

Abstract

Stereolithography is an additive manufacturing process, which makes it possible to fabricate useful complex 3D ceramic parts with a high dimensional resolution, a good surface roughness and properties close to those obtained by classical routes. Previous work concerning LTCC components, demonstrates that it is possible, by coupling the stereolithography with robocasting additive processes, to obtain multi-material components (e.g. ceramic / metal components). On the base of this previous work, the manufacturing of HTCC components using this innovative hybrid additive manufacturing process is described. Various complex and innovative geometries of HTCC alumina/tungsten components, in order to improve the characteristics of current circuits, are built and the mechanical and electrical properties characterized. Finally, hyper-frequency parameters of simulated HTCC complex micro strip resonators were compared to measured values on components manufactured by additive manufacturing.

Keywords

Additive manufacturing, stereolithography, robocasting, HTCC, Hyper-frequency

I. Introduction

The "Temperature Cofired Ceramic" multilayer technologies appeared around the beginning of the 90s. These processes consist in stacking ceramic dielectric sheets elaborated by tape casting, on which conductive patterns, resistances or capacities are printed by screen-printing. The different printed tapes are assembled and laminated to obtain multilayer circuits [1], [2]. Then metallized holes through different layers, called vias, allow connections between different conductive patterns through the dielectric layers (Figure 1).

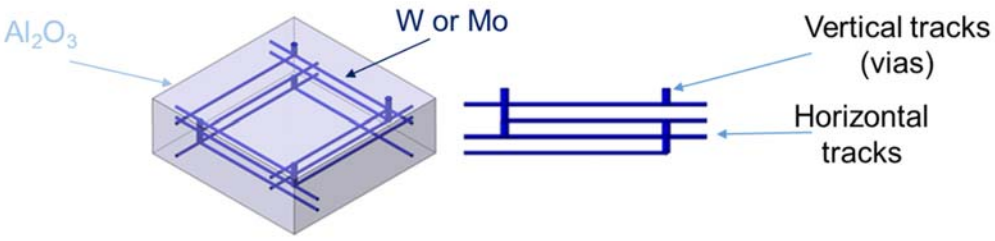

Figure 1 : Design of conventional HTCC component.

After lamination, the green stack is submitted to different heat treatments in a controlled atmosphere to eliminate organic components (debinding) and densify both ceramic and metallic materials (co-sintering). Co-sintering can be carried out at high temperature (T > 1000 °C) for High Temperature Cofired Ceramics (HTCC) or at low temperature (T ≤ 1000 °C) for Low Temperature Cofired Ceramics (LTCC). The choice of the sintering temperature will mainly depends on the conditions of use of the component, in particular the temperature. For instance, HTCC parts are used in the power assembly for aerospace [1]. HTCC materials commonly used in industry are alumina (dielectric substrate) coupled to tungsten or molybdenum (metallic tracks and vias) [1].

The conventional manufacture of HTCC and LTCC parts, i.e. tape casting for the substrate and screen-printing for the tracks and vias [3], limits some characteristics of the components:

1) The thickness of a ceramic layer must be typically larger than 150 microns in order to properly manipulating the tape-cast green sheet.
2) The shape of the metallic conductive pattern is limited to 2D patterns linked by vertical vias between dielectric layers, which limits the complexity of the metallic network and then the electrical functions than can be integrated inside the TCC component [1].
3) There is no possibility of developing lateral shielding.
4) It is impossible to make slanted vias.

In this context, the present work proposes the use of an hybrid additive process, already used in a previous work concerning LTCC materials [4], to manufacture complex HTCC components impossible to obtain by conventional routes.

Indeed, as presented in the previous article concerning LTCC components [4], additive manufacturing processes make it possible to automate production, to build more complex 3D metal circuits, more complex ceramic packaging shapes and to decrease the thickness of each layer. Moreover, additive manufacturing processes gives access to specific architectures to improve properties or to introduce new functions with the deposition of the desired material on

each voxel of the part during its construction. In addition, these processes allow the reduction of production costs because they do not require tooling and limit the loss of raw material.

II. Experimental

II.1 Hybrid machine and HTCC geometries

This hybrid machine designed and developed at laboratory is composed of a robotic arm, which controls the position of an extrusion head, coupled to a stereolithography device, as shown in Figure 2. The stereolithography equipment is supplied by 3DCeram Sinto (Limoges, France). The polymerization is achieved by a top-down laser beam (355 nm, 0 to 2000 mW) deflected by a XY galvanometric head.

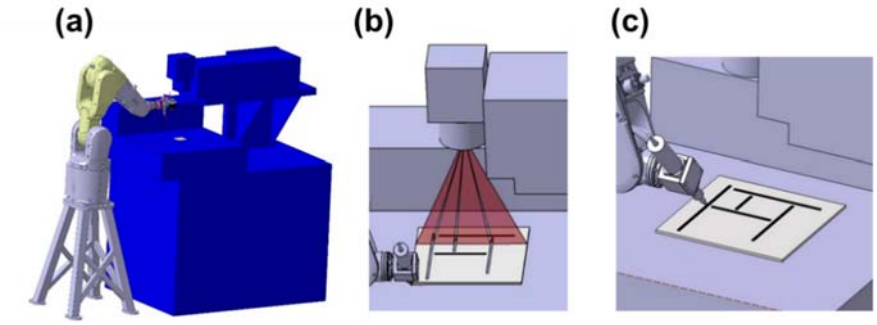

Figure 2: Assembly for the production of bi-material objects combining robocasting and stereolithography processes [4], [5].

This assembly represented Figure 2.a. contains on the right, the stereolithography equipment for printing the ceramic layers (Figure 2.b.) and, on the left, the robotic arm carrying the robocasting head to deposit the metallic patterns (Figure 2.c.).

The strategy chosen to manufacture a complex HTCC component is to decompose the manufacturing of this part in different steps of graduated complexity of the printed shapes (Figure 3). The final target is to build in one-step the final part. For each step of difficulty, the ceramic substrate is printed using the SLA device and a laser power lower than 200 mW. The alumina feedstock is supplied by 3DCeram Sinto (Limoges, France). The alumina powder loading is 57 vol% dispersed in an acrylic curable resin.

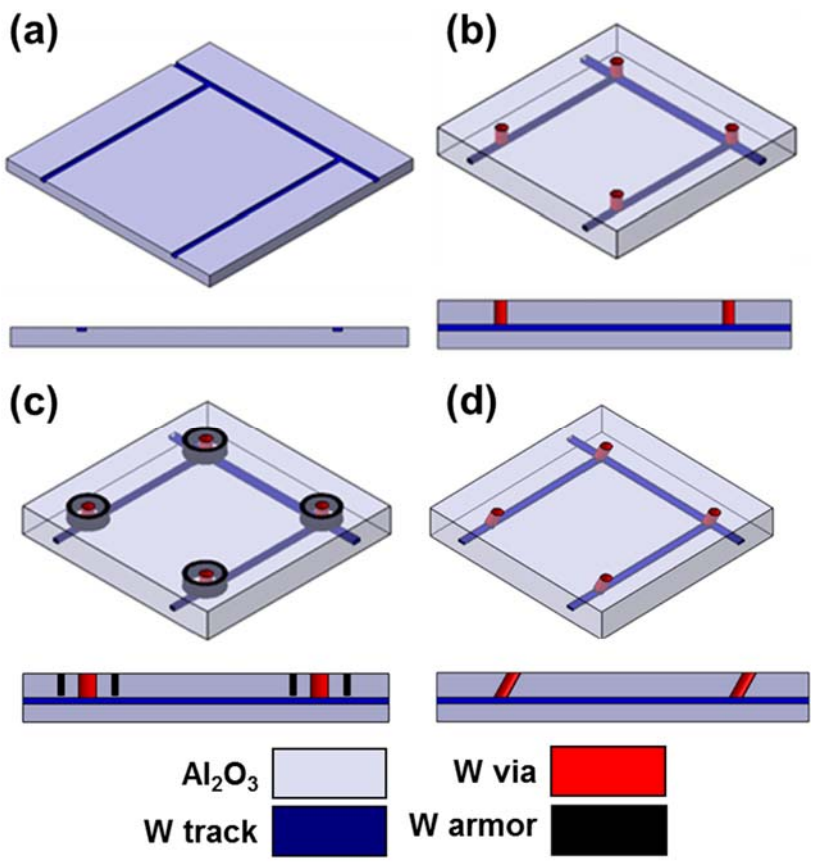

Figure 3: Presentation of different geometries studied: (a) Uncovered tracks, (b) Embedded tracks connected to the surface by vias, (c)
Arrmored vias and (d) oblique vias. The metal is represented in dark blue, the substrate in light grey, vias in red and armor in black.

The first step consists in the deposition of a metallic line on a ceramic substrate (Figure 3.a.). The motif is defined in order to measure the conductivity of the track by the 4-points method and to observe its morphology after co-sintering. The second step proposes to embed the track between two ceramic layers in order to evaluate the co-sintering between metal and ceramic materials and connect these tracks to the surface by vias (*Figure 3*.b.). The quality of the co-sintering was evaluated by the densification of both alumina substrate and metallic track, by eventual delamination at alumina/tungsten interfaces on SEM observations and by the conductivity of the metallic track. This geometry aims to validate the feasibility of vias and their connection with the track. The conductivity of the metallic circuit will be measured after co-sintering. The next two geometries cannot be obtained using conventional methods and correspond to a significant improvement in the performance of HTCC components. The third geometry corresponds to continuous armored vias (*Figure 3*.c.). The last geometry (*Figure 3*.d.) consists in the realization of oblique vias which allow to connect two tracks with an x and/or y shift.

Two final geometries are considered in order to characterize developed materials in hyper-frequency range (Figure 4). We have chosen resonant structures because they allow characterizing dielectric and metallic materials in a precise way.

The first geometry (Figure 4.a. and 4.b.) is a microstrip structure where the metal tape is placed on the dielectric substrate. The microstrip resonator (blue) is composed of three lines and a ground plane (black). Simulated vias (Figure 4.a.) are replaced by the construction of continuous walls (Figure 4.b.) and should provide more accurate results.

The second geometry (Figure 4.c. and d.) is also a microstrip resonator, but the metal tape is placed between two dielectric layers. This geometry consists of a surface ground plane (in black) with, on both sides, coplanar access for measurement by microwave probes. The line, embedded in the dielectric substrate, is a half-wave resonator coupled to the coplanar access by evanescent modes. The analysis of the resonances (frequencies and quality factors) will make it possible to characterize the structure.

The distribution of the electromagnetic field in the both structures is different which allows, by retro-simulation, to evaluate the dielectric and metallic losses. These parts have been designed in order to produce optimal performances and have been qualified by retro-simulation at high frequencies (1-10 GHz).

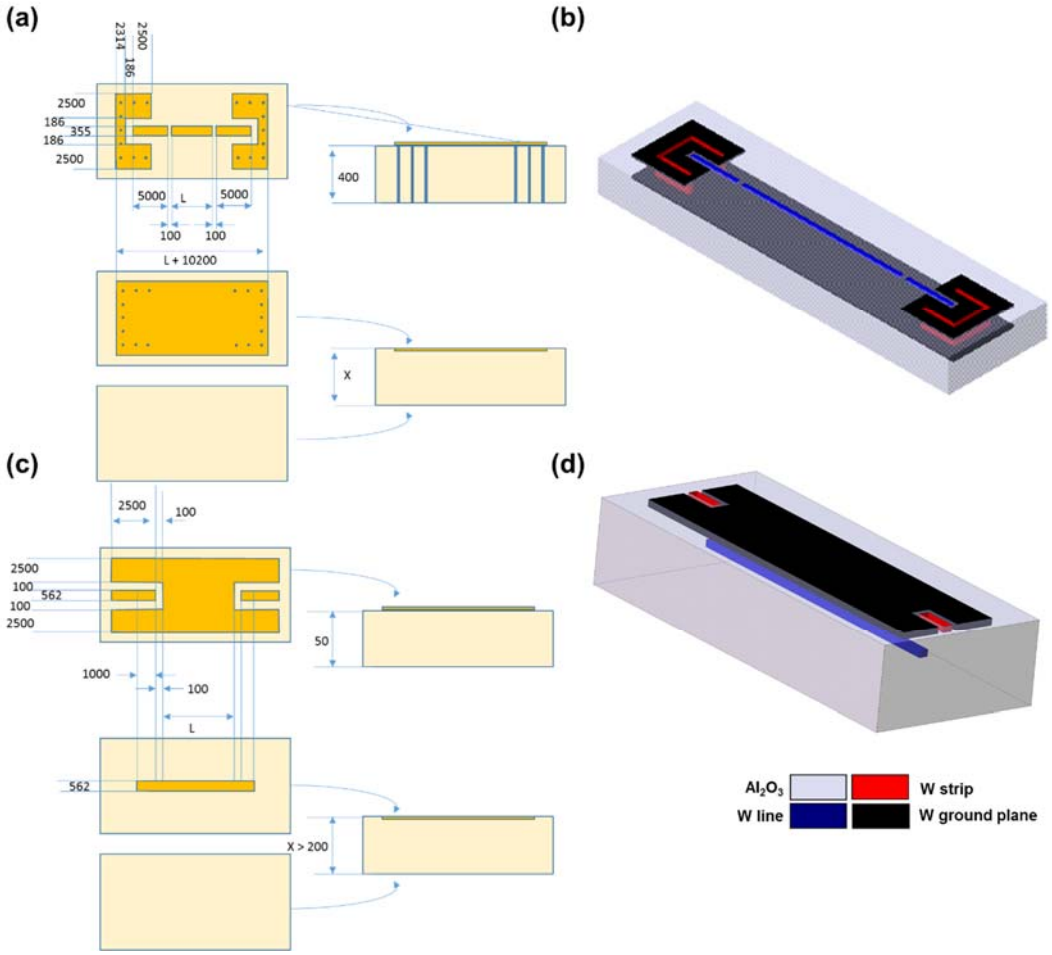

Figure 4: Original geometries for hyper frequency characterization: a microstrip resonator (a. and b.) and an embedded microstrip resonator (c. and d.) with the dimensions given in micrometre.

The microwave behaviour simulations were carried out using Momentum software (Keysight Technologies). The results of the simulations determine the parameters S_{11} and S_{21}, respectively the reflection and transmission parameters as a function of the signal frequency (Figure 5).

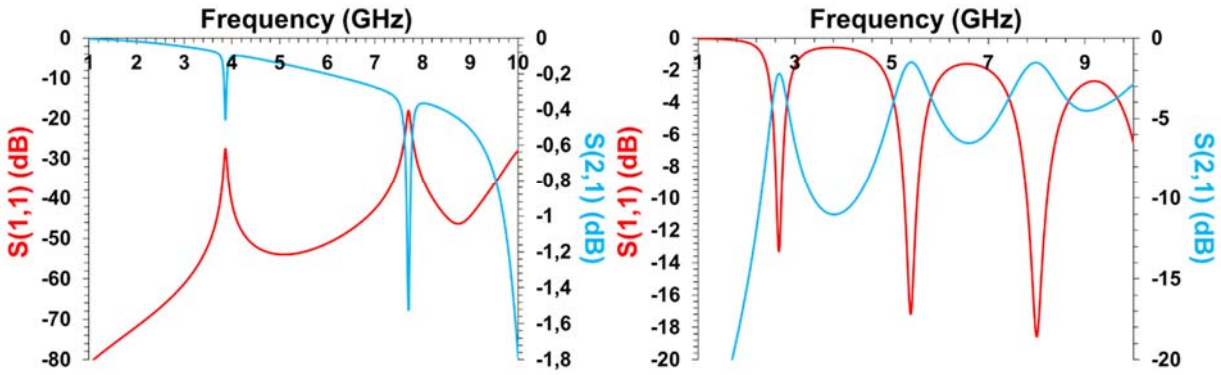

Figure 5: Simulated microwave behaviour of (a) microstrip resonator and (b) embedded microstrip resonator.

For the microstrip resonator, the simulation predicts two resonance peaks at 3.9 and 7.8 GHz with a respective intensity of -0.4 and -1.5 dB for the transmission parameter. In the case of the embedded microstrip resonator, the simulation predicts three peaks of resonance at 2.6, 5.2 and 7.4 GHz with an intensity around -2 dB for the transmission parameter.

Theses geometries have been build using the hybrid additive process and then characterized in the microwave range. The printing parameters of the alumina substrate are a laser power lower than 200 mW, a laser velocity comprised between 1 and 4 m/s and a hatching space lower than 50 µm. Concerning the robocasting process, a printing speed near 10 mm/s was used. The standard accuracy obtained by the robocasting process is about 40 µm. The challenge is here to obtain parts for which the dimensions are as close as possible to those designed by the simulation. The choice of the materials to reach the expected properties in the microwave is of course essential.

II.2 Ceramic paste for dielectric substrate

The ceramic materials used in the HTCC technology are alumina, zirconia or even mulitte [1], [3], [6], [7]. Alumina is a material conventionally used for stereolithography and hyperfrequency applications. So a fine reactive α-alumina powder is chosen to prepare the ceramic paste for stereolithography (P172LSB, Altéo, France, d_{50} = 0.4 µm, Specific Surface Area BET = 8 m²/g, purity = 99.80 %). The granulometry makes it possible to deposit very thin layers (from 10 to 50 µm) during the stereolithography process and the purity leads to suitable dielectric properties (permittivity and loss) at high frequencies. The formulation of the stereolithography suspension was carried out and supplied by 3DCeram-Sinto company (Limoges, France)

II.3 Metallic paste for tracks and vias

The metallic tracks and vias ensure the conduction of the current in the component. The metallic materials used in the case of HTCC technology are tungsten, molybdenum or

even palladium [1], [3], [8]. According to the process, the particle size of the metallic powder and the rheology of the paste must allow extrusion through a 100 µm diameter nozzle. Indeed, the track width and vias diameter target are both around 100 µm after sintering. In this respect, a tungsten powder with a mean particle size of about 1.1 µm and quasi-spherical grains (AW2110, Umicore, Belgium) was used (Fig. 6 and Table 1). The metallic paste is based on a cellulosic binder in aqueous media. The tungsten loading is equal to 39 vol%. The consolidation of the extruded paste is obtained by natural drying (about 30 min).

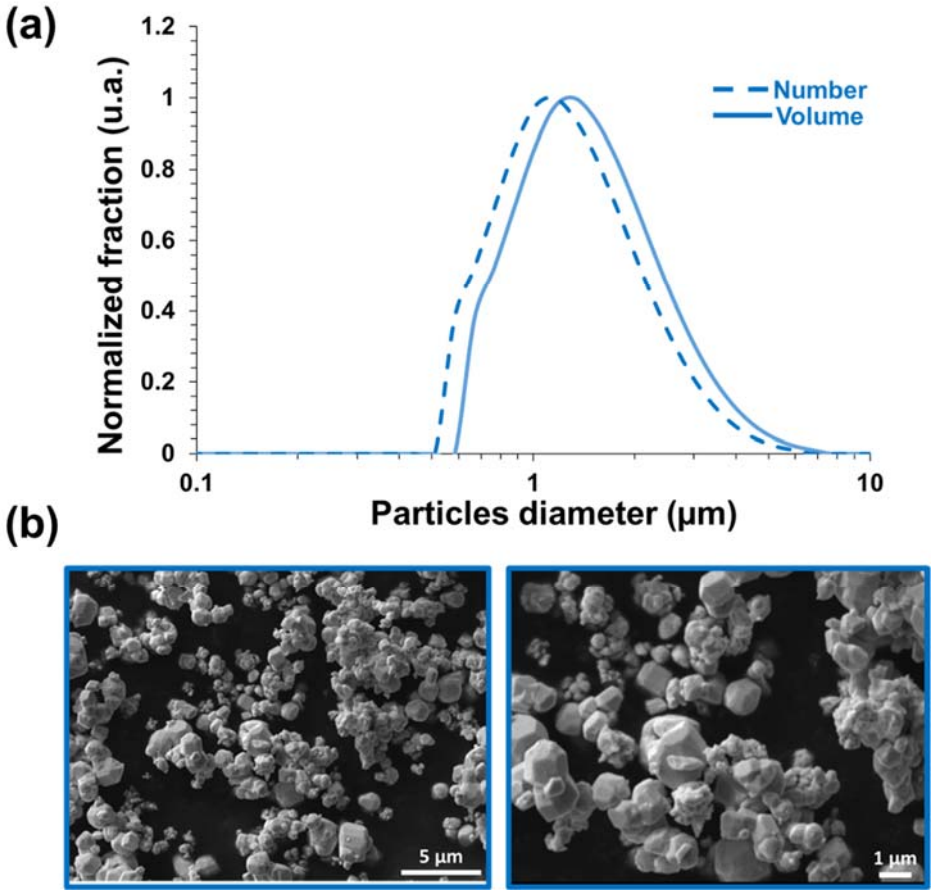

Figure 6: Granulometry curve (a) and micrographs of the tungsten powder (AW2110) (b).

Table 1: Characteristics of the tungsten powder.

Reference	d_{50} (µm)	Density	Specific surface BET (m^2/g)
AW2110	1.1	18.5	0.55

A paste containing 39 vol% (i.e. 92 wt%) tungsten, with a rheological behaviour adapted to the extrusion of filaments through a 100 µm diameter nozzle, was developed at laboratory (Figure 7).

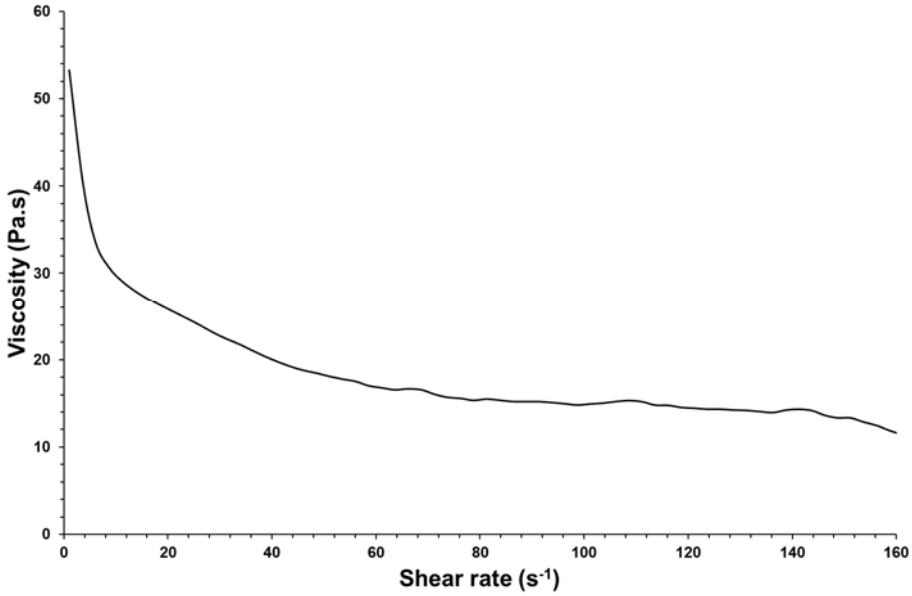

Figure 7 : Rheogramm of the robocasting tungsten paste.

III. Results and discussions

III.1 Printed parts

The alumina substrates are built by stereolithography with a layer thickness of 50 microns. The tracks are printed by robocasting with a printed speed of 10 $mm.s^{-1}$, a nozzle diameter of 100 µm and an area between the nozzle and the substrate of 50 µm. The vias and armors are obtained in two steps:

- Desired shapes of vias and armors are milled in the polymerized paste with a milling tool (diameter of 300 µm) and an air-powered spindle (80.000 rpm). The tools imposes the diameter of the vias and the width of the armors.
- Obtained shapes are filled with the tungsten paste by means of the micro-extrusion head.

For each studied geometry, five samples have been printed, heat-treated and characterised. Observations of tracks, vias and armored vias before thermal treatment are carried out by optical microscopy (Figure 8).

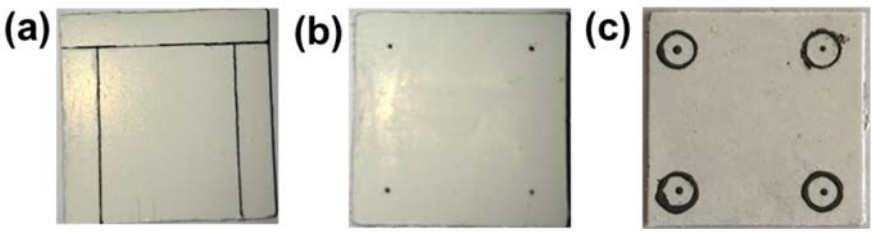

Figure 8: Micrograph of green parts (a) uncovered tracks, (b) Embedded tracks with vias and (c) Armored vias.

The tungsten green tracks have a width of 150 microns (Figure 8.a.) and vias a diameter of 300 microns (Figure 8.b.). Circle armors have diameter of 5 mm and a width of 300 microns (Figure 8.c.).The dimensional target values were lower (80 µm for the witdth of a track, the diameter of a via and the width of an armor). The accuracy is mainly limited by the robocasting device resolution.

Both the ceramic suspension for stereolithography and tungsten paste for micro-extrusion contain organic components (acrylic resin for the alumina paste and ethylcellulose for the tungsten paste). It is then necessary to determine the appropriate thermal cycles for the debinding of printed parts with the challenge to minimize carbon residues while avoiding the oxidation of the tungsten.

III.2 Debinding

A critical step of the process of HTCC manufacturing is the co-debinding and the co-sintering of ceramic/metal parts. The thermal cycle requires to eliminate the totality of the organic components without any cracking, deformation or delamination and to obtain a dense part. Both the alumina stereolithography suspension and the tungsten extrusion paste were first characterized by TGA under air atmosphere (Thermogravimetric Analysis - Labsys-evo-1600, Setaram, France) (Figure 9).

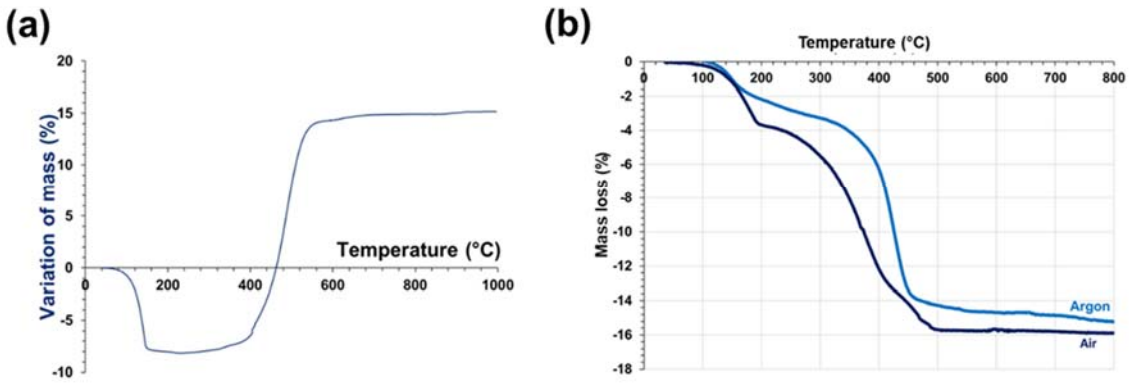

Figure 9: Thermal analysis of a) tungsten paste of robocasting under air and b) alumina suspension of stereolithography under air (dark blue curve) and under argon (blue curve).

The TGA of the metal paste (Figure 9.a) under air shows a total loss of mass which reaches about 8 % up to about 250°C, corresponding to the organic phase in the robocasting paste (61 vol%, i.e. 8,1 m%). For temperatures higher than 250°C, the weight gain corresponds to the oxidation of the metal that is confirmed by XRD analysis (Figure 10). The

raw tungsten powder is metallic (ICDD file 00-004-0806) and the powder calcined at 800 °C under air is tungsten trioxide (WO_3) (ICDD file 00-043-1035).

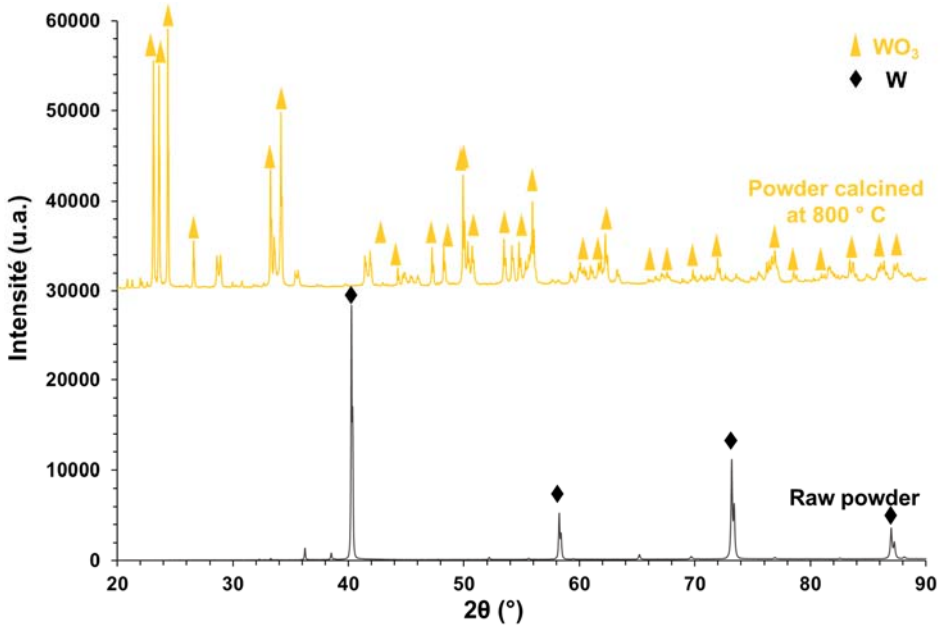

Figure 10: XRD pattern of a) raw tungsten powder (black) and b) powder calcined at 800 °C under air (yellow).

The oxidation of tungsten during debinding under air is detrimental and causes the part breaking and/or fissuration caused by an important expansion of the material.

To overcome this problem, the debinding of HTCC components has to be performed under neutral or reducing atmosphere. But, as showed in Figure 9.b, the elimination of the organic phase from the alumina stereolithography suspension is more complete under air than under reducing atmosphere with a mass loss of 15 % under air, which corresponds to the organic concentration in the suspension (i.e. 39 vol%), against 13.5 % under reducing atmosphere. Then a large amount of carbon remains in the part debinded under neutral atmosphere as confirmed by the grey or black colour of the surface of the part after treatment at 800°C under argon (Figure 11).

Figure 11: Alumina part obtained by stereolithography and debinded under argon at 800°C for 3 hours.

To improve the organic extraction in reducing atmosphere, the use of a wet debinding atmosphere was used [9], [10] by introducing water in the argon/H_2 gas. Different partial water pressures into the debinding atmosphere were tested in order to found a good compromise between a complete removal of carbon residues and a non-oxidation of the tungsten. The partial water pressure selected for the debinding is then fixed between 900 and 2300 Pa at 35°C depending on the dimensions of the parts. This debinding procedure under wet reducing atmosphere allows, in one hand to recover a white part, which attest of a very low concentration of residual carbon and, in a second hand, to avoid the oxidation of tungsten.

III.3 Alumina sintering

The alumina has to be fully densified in order to confer high dielectric properties, especially at high frequencies, and also suitable mechanical properties. Dilatometric analysis (TMA1750, Setaram, France) were performed on alumina samples manufactured by stereolithography after debinding (Figure 12).

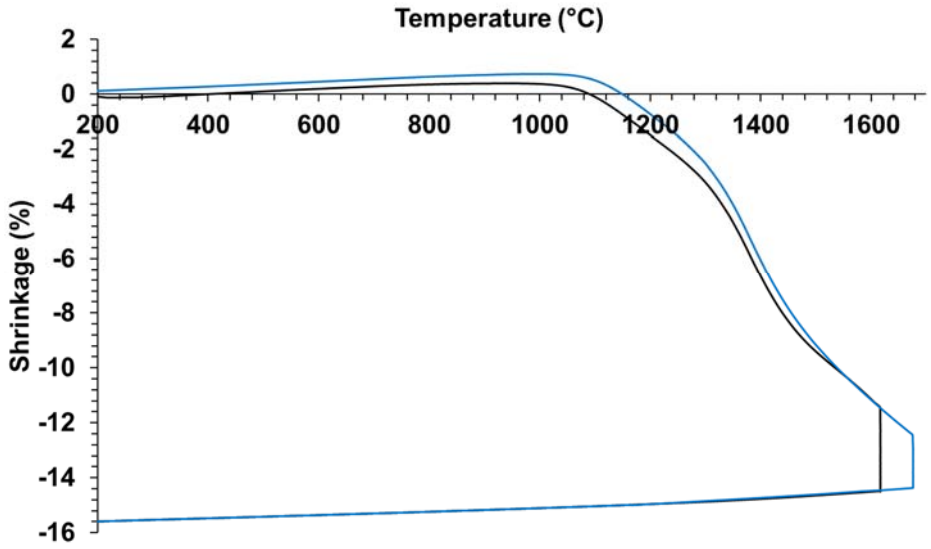

Figure 12: Dilatometry of alumina substrate at 1600 °C (black curve) and 1650 °C (blue curve) for 3h under air, 5°C/min.

The same final linear shrinkage was recorded for sintering at 1600 and 1650°C during 3h, of about 15.6 %. The microstructures of sintered samples were observed by SEM (JEOL JSM-IT-300-LV) (Figure 13). Grain growth is logically larger at 1650°C but no exaggerated one with acicular grains takes place, even for sintering at 1650°C.

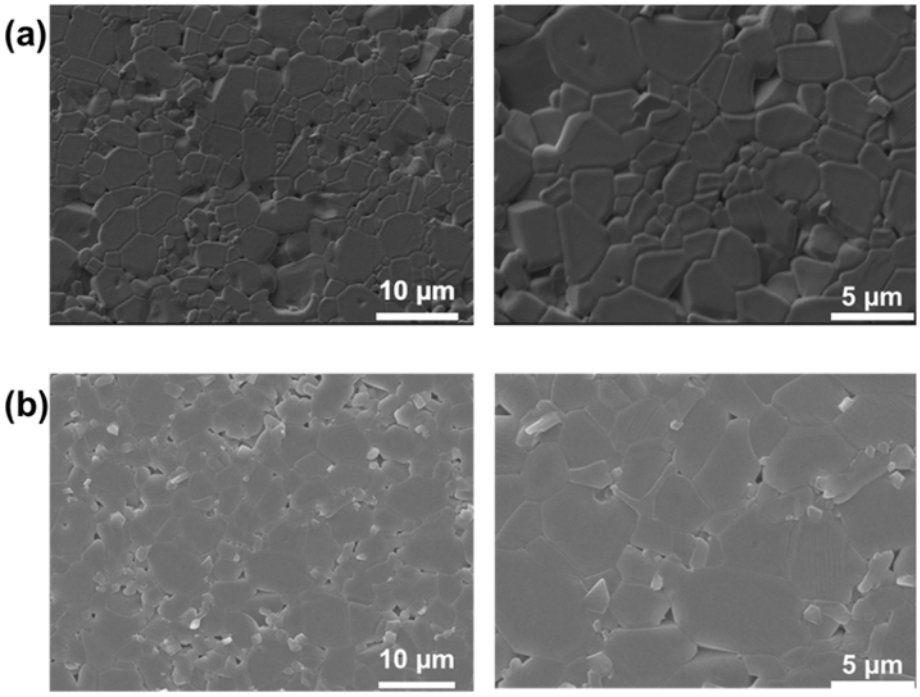

Figure 13: Micrograph of sintered alumina at a) 1600 and b) 1650 °C for 2 hours under air.

The relative density of the HTCC substrates, measured by the Archimedes' method using ethanol as the inhibiting liquid, are reported in the Table 2. The sample used are cylindrical with a diameter equal to 8mm and a length equal to 4 mm. For each measure, 10 samples are tested in order to obtain a representative mean value.

Table 2: Relative density of HTCC substrate sintered at 1600 and 1650 °C in air for 2 hours.

	Relative density (%)
1600 °C / 2 h	97
1650 °C / 2 h	98

For both sintering temperatures, the relative density is close to the theoretical density. The choice of the sintering temperature will therefore be made according to the mechanical properties of the substrate and the electrical conductivity of tungsten tracks.

III.3 Tungsten sintering

In order to define the tungsten sintering temperature, a comparison of the microstructure and of the resistivity of three track sintered at 1600 and 1650°C during 2 hours was performed [11].

Tungsten tracks have a higher conductivity (resp. lower resistivity) when sintered at 1650°C (Table 3) (measured on 5 samples at each sintering temperature). Then, the sintering temperature of the manufactured multimaterial parts was fixed at 1650°C during 2 hours. The final conditions of debinding and sintering are summarized in Figure 14.

Table 3: Resistivity of tungsten tracks sintered at 1600 and 1650 °C for 2 hours in reduced atmosphere (Ar/2%H_2).

	Track resistivity (Ω.m)
1600 °C / 2 h	$7{,}9.10^{-7}$
1650 °C / 2 h	$6{,}5.10^{-7}$

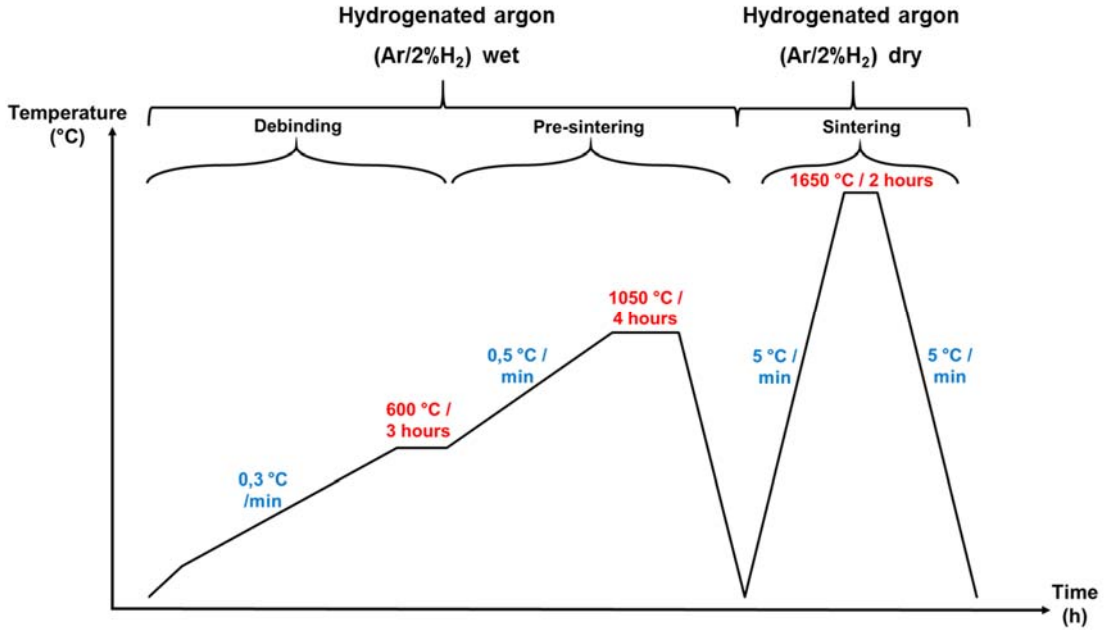

Figure 14: Thermal cycle for debinding and sintering of HTCC parts under reducing atmosphere (Ar/2%H_2).

The debinding is performed in a wet reducing atmosphere (Relative humidity = 35% at 35 °C) in order to eliminate organics while avoiding oxidation of the metallic patterns and the sintering in dry reducing atmosphere (Ar/2%H_2). These thermal cycles allows obtaining different geometries consisting in dense alumina dielectric material associated to tungsten metallic conductor (Figure 15).

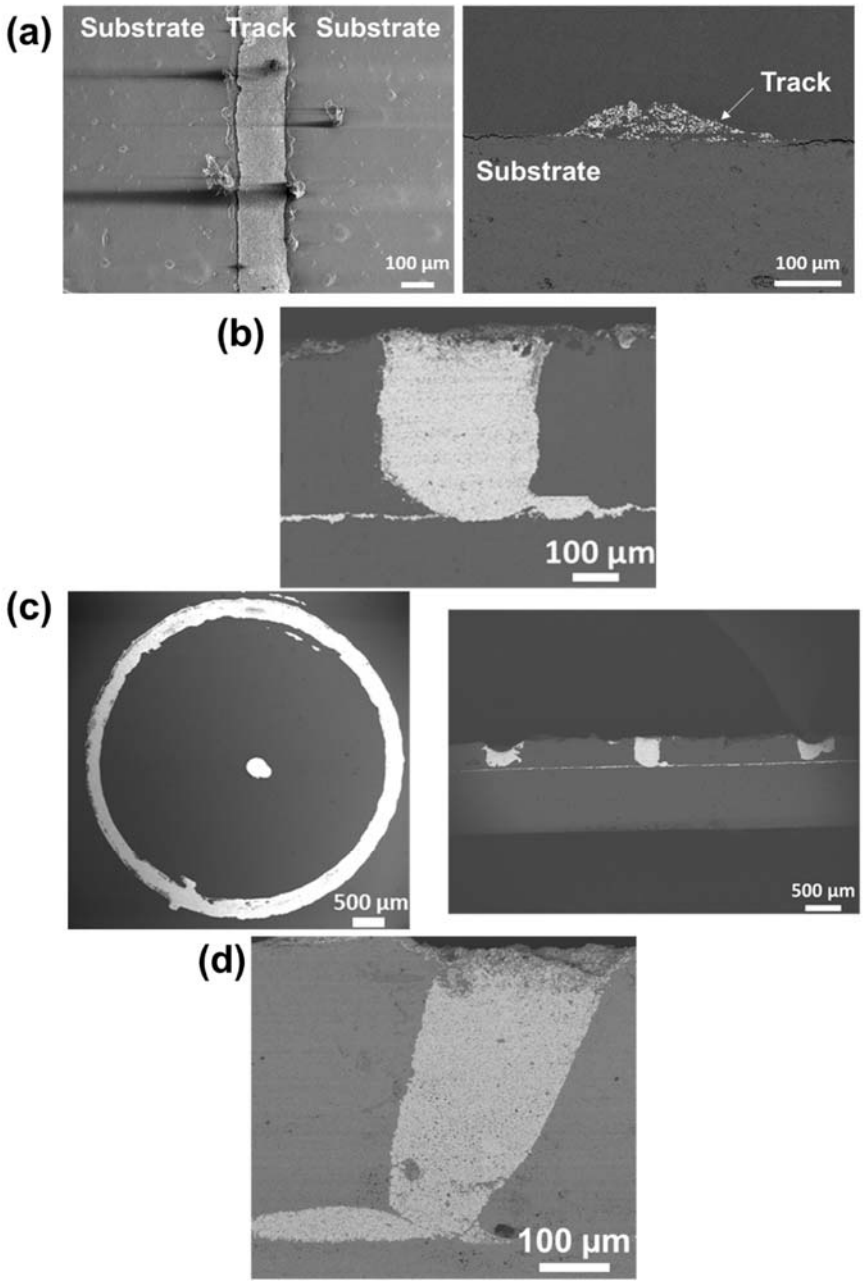

Figure 15: SEM images of HTCC components: a) uncovered tracks, b) embedded track connected to surface by vias, c) armored vias, and d) oblique vias after heat treatments given in figure 14.

The observation of each picture in Figure 15 show that all the proposed designs have been correctly printed and heat-treated. In pictures Figure 15 b, c (right) and d, the horizontal lines are tungsten tracks connected to a vertical via. The uncovered tungsten tracks have a width of 150 µm and a thickness of 40 µm (Figure 15.a). Vias have a diameter of 270 µm and a depth of 300 µm (Figure 15.b). A circular tungsten armor was printed around a via (Figure 15.c), in order to improve the performance of current circuits. The diameter of the armor is 4.4 mm, a width of 270 µm and a depth of 300 µm. The oblique via (Figure 15.d), makes it

possible to avoid several vertical and horizontal transitions to connect two tracks shifted along the x, y and z-axis, has a diameter of 270 µm and a depth of 300 µm.

III.4 Mechanical characterizations

The mechanical properties of the sintered alumina substrate are measured using 4-point bending test. The Young's modulus E is determined using the classical theory of beams (Equation 1):

$$E = \frac{F_{max}\, L^3}{8bh^3\Delta y} \qquad \text{Eq. 1}$$

where Δy is the displacement of the machine, L the distance between bottom supports (40 mm) and l (20 mm) the distance between upper supports, b and h the width and the thickness of beam respectively, and F the maximal load at rupture. The Young modulus values given in Table 4 are in agreement with the characteristics usually reported in the literature for a HTCC dielectric substrate [12]–[14].

Table 4: Young Modulus of the alumina dielectric substrate after sintering at 1600 and 1650 °C for 2 h (Ar/3%H_2). Average on 10 samples.

HTCC substrate	Young modulus E (GPa)
1600 °C/2 h	297 +/- 18
1650 °C/2 h	290 +/- 7

III.5 Electrical resistivity

The experimental electrical resistance of the tracks was measured by the 4-points method on the first geometry (Figure 3 a). For more precision of the measurement, a platinum wire was bond with a platinum paste to the places where the measures have to be done. The resistivity, ρ_{track} , of the tracks is calculated using equation 2:

$$\rho_{track} = \frac{R \times S}{l} \qquad \text{Eq. 2}$$

where l and S are the length and the section of the track respectively, and R the measured resistance.

In both cases of uncovered tracks and embedded tracks with vias (Figure 3.b), similar resistivity values of $6.97.10^{-7}$ Ω.m, for a line length of 20 mm and a sintering temperature of 1650°C, were measured. The embedding of the tungsten track inside the alumina dielectric

part does not induce a decrease of the conductivity that suggests that the embedded track is not damaged and the vias are well aligned with the tracks.

III.6 High frequency characterizations

Examples of manufactured parts are shown in figure 16, together with the original geometries given in figure 4, in order to compare the dimensions.

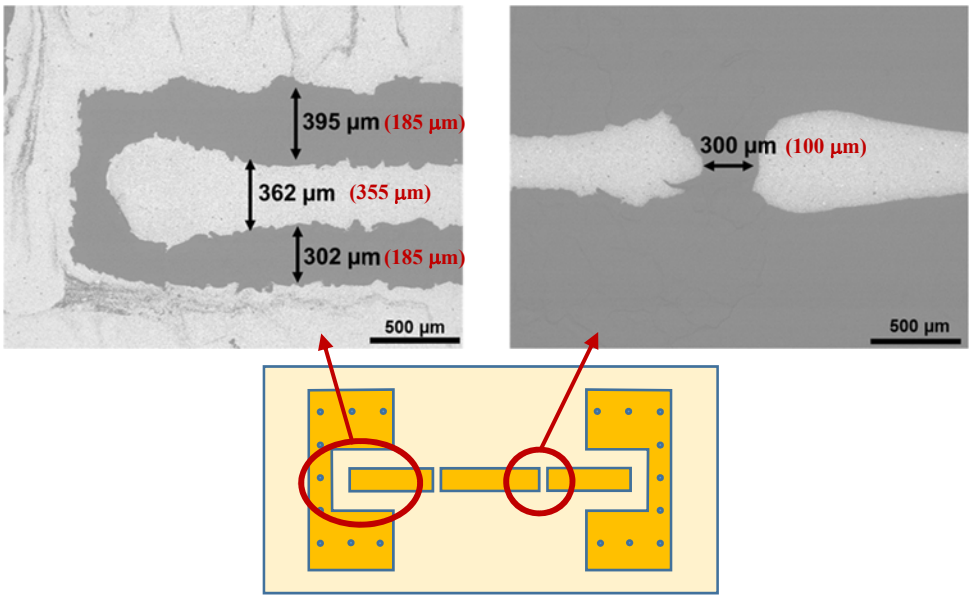

(a) microstrip structure

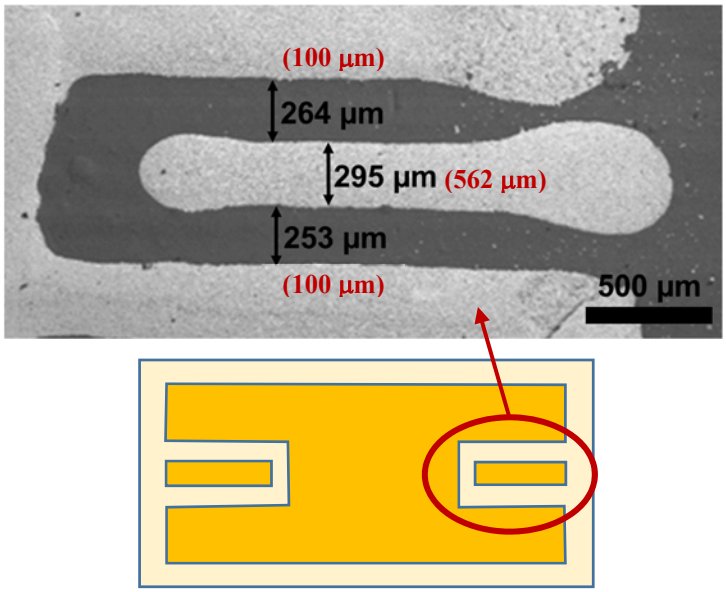

(b) embedded microstrip structure

Figure 16: Micrograph of the upper side of the two structures produced. The dimensions after manufacture, in black, are compared to the dimensions used by the simulation, in red.

The dimensions of the metallic tracks are relatively different from those of the simulation due to the limitations of the robot's positioning system, which is ± 20 microns and more precisely the Z positioning of the nozzle with respect to the surface of the substrate. Moreover, the gap between the line and the ground plane is also different to the simulation caused by the creation of a droplet at the beginning of the line, which changes the dimensions of the metal strips. For measurement at microwave frequencies, these modified dimensions create an impedance mismatch between the measurement system and the circuit, which degrades the results. Nevertheless, it was possible to analyze the microwave response of the samples and compare results to the simulation (Figure 20).

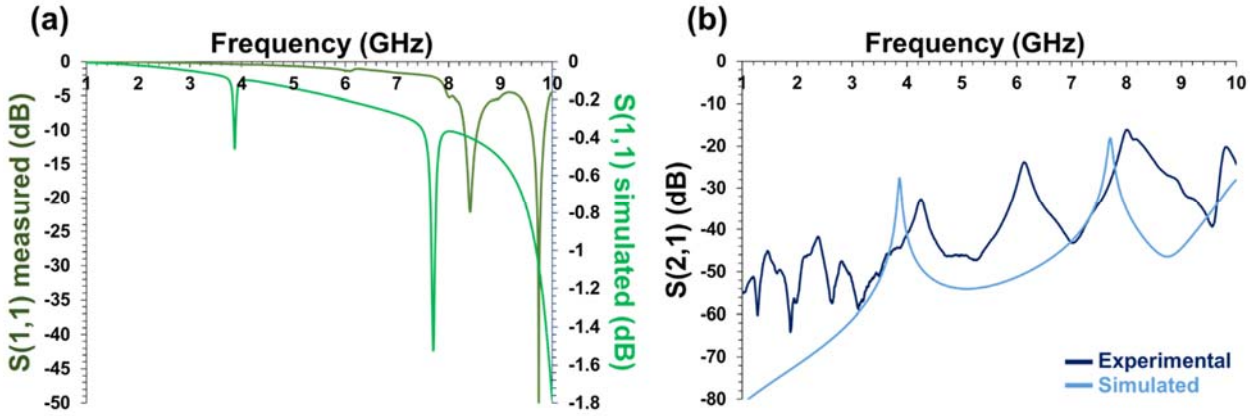

Figure 17 : Comparison of simulated and experimental reflexion (a) and transmission (b) parameters for a HTCC microstrip resonator sintered at 1650 °C for 2h under reducing atmosphere.

The frequency behaviours do not exactly correspond to the simulation. Concerning the transmission parameter S_{21} (Figure 17.b), five resonance peaks are observed at 1.5, 2.4, 4.26, 6.13 and 8.00 GHz while the simulation predicted only two peaks at 3.9 and 7.8 GHz. These additional peaks at 1.5, 2.4 and 6.13 GHz can be attributed to the low thickness of the substrate and would therefore be parasitic peaks. In addition to dimensions problems, one of the causes of this difference between simulation and measurement can be attributed to the presence of the metallic plane imposed by the measurement device (Figure 18). During the measure, the lower dielectric is placed between the ground plane of the circuit and the metallic surface of the measurement bench. It constitutes a planar guide in which a part of the wave can propagate and disturb the behavior of the microstrip resonator. This disturbance is as more important as the thickness of the lower dielectric is high.

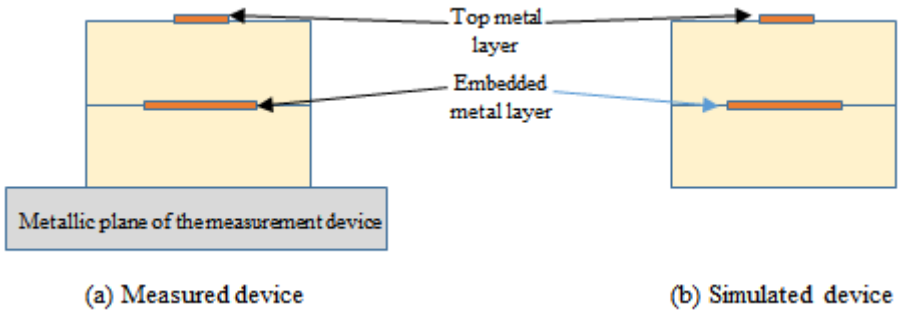

Figure 18: Comparison of the measured device (a) and the initial simulated device (b)

The simulation was then modified, by taking into account this metallic plane of the measuring device (Figure 19), and becomes closer to the experimental measurements. The two curves show the same number of peaks with close intensity but with a frequency shift. The five peaks of resonance at 3.3, 3.9, 4.9, 6.4 and 7.8 GHz, where the peaks at 3.3, 4.9 and 6.4 are parasitic peaks due to the metallic plane of the measuring device.

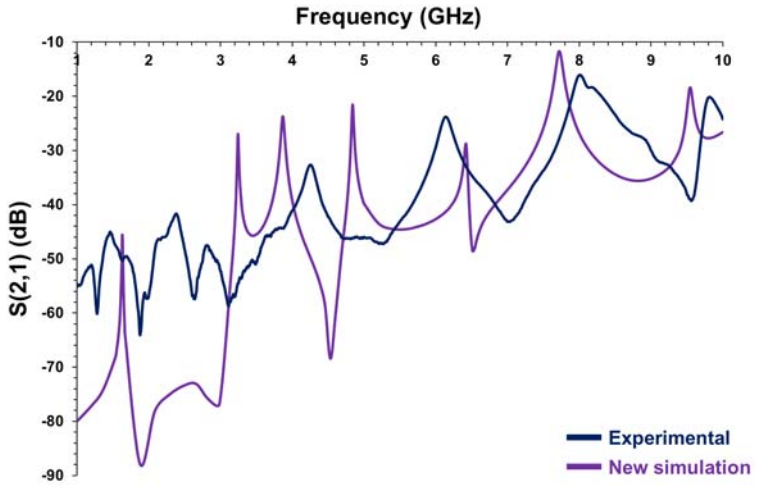

Figure 19 : Comparison of the new simulation and the measure experimental parameter of transmission for a HTCC microstrip resonator sintered at 1650 °C for 2h under reducing atmosphere.

For the second geometry, embedded microstrip resonator, the same analyze was conducted (Figure 20).

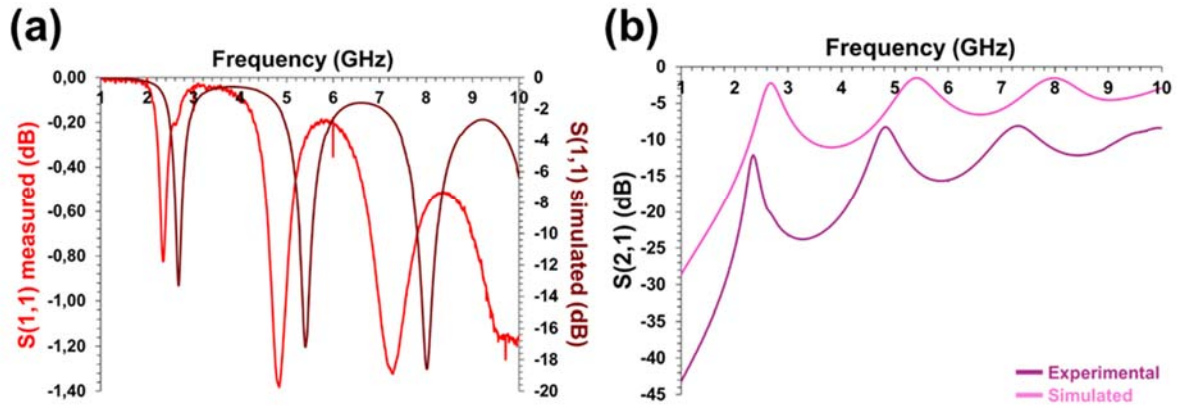

Figure 20 : Experimental frequency response curves of a HTCC embedded microstrip resonator sintered at 1650 °C for two hours under a reducing atmosphere.

In this configuration, the simulated and the experimental curves have the same shape. Indeed, for the reflexion and transmission parameters, three peaks of resonance are observed at 2.8, 5.6 and 7.9 GHz. However, we can notice a slight shift in terms of frequency and intensity of the resonance peaks between the simulation and the experimental results. The frequency shift is probably due to the difference between the simulated and experimental dimensions of the metallic patterns. The intensity shift is due to the difference between the simulated and experimental thicknesses between the embedded line and the surface of the sample.

IV. Conclusions

An innovative additive hybrid machine has been used to manufacture alumina/tungsten HTCC components. This hybrid machine makes it possible to build parts consisting in an alumina dielectric substrate, realized using a stereolithography process, and tungsten electrical conductor tracks deposited by robocasting.

A specific debinding cycle under wet reducing atmosphere was defined in order to reach a complete removal of carbon and to avoid the oxidation of tungsten in the HTCC components fabricated using this hybrid additive machine. The mechanical properties of the dense dielectric alumina, co-sintered with tungsten under reduced atmosphere up to 1650 C for 2 hours, are close to those obtained by conventional methods with a Young modulus E = 280 ± 11 GPa.

The metal tracks have a minimum width of 110 microns and a maximum thickness of 40 microns after co-sintering. Their resistivity is about $6.9.10^{-7}$ Ω.m, corresponding to expectations for a hyper-frequency applications. Various multimaterial parts with more or less complex

geometries were manufactured, from the track deposited onto an alumina substrate to a complex micro strip resonators.

Hyper-frequency characterizations show that it is possible to manufacture electronic components using this additive hybrid machine. Nevertheless, the dimensional accuracy (width and thickness) of the deposited metal tracks, as well as their positioning on the alumina substrate must be improved. In this respect, we will modify the positioning system of the micro-extrusion nozzle.

[1] C. Robert, “Fiabilité des assemblages de puissance,” Thèse de l’Université de Paris-Saclay, 2015.
[2] W. Bakalski *et al.*, “5-6.5 GHz LTCC power amplifier module with 0.3 W at 2.4 V in Si-bipolar,” *Electronics Letters*, vol. 39, no. 4, Feb. 2003, doi: 10.1049/el:20030249.
[3] H. D. Smith and D. F. Elwell, “HTCC/LTCC use of multiple ceramic tapes in high rate production,” US5318820A, Jun. 1994.
[4] J. Raynaud *et al.*, “Hybridization of additive manufacturing processes to build ceramic/metal parts: Example of LTCC,” *Journal of the European Ceramic Society*, vol. 40, no. 3, pp. 759–767, Mar. 2020, doi: 10.1016/j.jeurceramsoc.2019.10.019.
[5] J. Raynaud, “Elaboration de pièces 3D multimatériaux par fabrication additive,” thesis, Limoges, 2019.
[6] W. Li, A. Feingold, P. Palanisamy, and G. Lorenz, “Co-sintering Zirconia Electrolyte and Insulator Tapes for Sensor Applications,” *J. Am. Ceram. Soc.*, vol. 95, no. 12, pp. 3815–3820, Dec. 2012, doi: 10.1111/jace.12044.
[7] Q. L. Tan *et al.*, “Zirconia ceramics applied in a pressure-sensitive device fabricated using HTCC technology,” *Sensors and Materials*, vol. 26, no. 1, pp. 19–30, 2014.
[8] L. Mele *et al.*, “A molybdenum MEMS microhotplate for high-temperature operation,” *Sensors and Actuators A: Physical*, vol. 188, pp. 173–180, Dec. 2012, doi: 10.1016/j.sna.2011.11.023.
[9] A. J. Blodgett and D. R. Barbour, “Thermal Conduction Module: A High-Performance Multilayer Ceramic Package,” *IBM Journal of Research and Development*, vol. 26, no. 1, pp. 30–36, Jan. 1982, doi: 10.1147/rd.261.0030.
[10] J. Bolitschek, S. Luidold, and M. O’Sullivan, “A study of the impact of reduction conditions on molybdenum morphology,” *International Journal of Refractory Metals and Hard Materials*, vol. 71, pp. 325–329, Feb. 2018, doi: 10.1016/j.ijrmhm.2017.11.037.
[11] V. I. Torbov, V. N. Troitskii, T. V. Rezchikova, A. Z. Rakhmatullina, A. P. Zuev, and V. N. Doronin, “Sintering of very fine molybdenum and tungsten powders,” *Powder Metall Met Ceram*, vol. 21, no. 1, pp. 42–45, Jan. 1982, doi: 10.1007/BF00791724.
[12] A. Khalil, “Technologies LTCC et stéréolithographie céramique 3D appliquées à la conception de dispositifs millimétriques et sub-millimétriques,” 2010.
[13] L. Golonka, “Technology and Applications of Low Temperature Co-Fired Ceramic (LTCC) Based Sensors and Microsystems,” *BULLETIN OF THE POLISH ACADEMY OF SCIENCES TECHNICAL SCIENCES*, vol. 54, Jun. 2006.
[14] H. Jantunen, T. Kangasvieri, J. Vähäkangas, and S. Leppävuori, “Design aspects of microwave components with LTCC technique,” *Journal of the European Ceramic Society*, vol. 23, no. 14, pp. 2541–2548, Jan. 2003, doi: 10.1016/S0955-2219(03)00155-9.